RSC Advances

PAPER

View Article Online
View Journal | View Issue

Cite this: *RSC Adv.*, 2023, **13**, 4040

New iron(III) complex of bis-bidentate-anchored diacyl resorcinol on a Fe_3O_4 nanomagnet: C–H bond oxygenation, oxidative cleavage of alkenes and benzoxazole synthesis †

Mona Majedi, [a] Elham Safaei *[a] and Sašo Gyergyek [b]

We have synthesized a novel, bis-bidentate, covalently anchored, 4,6-diacetyl resorcinol (DAR) ligand on silica-coated magnetic Fe_3O_4 nanoparticles and the corresponding bi-metallic iron(III) complex (Fe_3O_4@SiO_2-APTESFe_2L^{DAR}). Both the chemical nature and the structure of the homogeneously heterogenized catalyst were investigated using physico-chemical techniques. The results obtained by XPS, XRD, FT-IR, TGA, VSM, SEM, TEM, EDX, ICP and AAS revealed a magnetic core, a silica layer and the grafting of a binuclear iron complex on the Fe_3O_4@SiO_2-APTES, as well as its thermodynamic stability. Despite many reports of metal complexes on different supports, there are no reports of anchored, bi-metallic complexes. To the best of our knowledge, this is the first report of a bi-active site catalyst covalently attached to a support. This study focuses on the catalytic activity of an as-synthesized, bi-active site catalyst for C–H bond oxygenation, the oxidative cleavage of alkenes, and the multicomponent, one-pot synthesis of benzoxazole derivatives with excellent yields from readily available starting materials. Our results indicated high conversion rates and selectivity under mild reaction conditions and simple separation using a magnetic field. The leaching and recyclability tests of the catalyst were investigated for the above processes, which indicated that all the reactions proceed *via* a heterogeneous pathway and that the catalyst is recyclable without any tangible loss in catalytic activity for at least 8, 5 and 5 cycles for C–H bond oxygenation, C=C bond cleavage and benzoxazole synthesis, respectively.

Received 28th October 2022
Accepted 17th January 2023

DOI: 10.1039/d2ra06818d

rsc.li/rsc-advances

Introduction

Schiff base ligands and especially their metal complexes are widely used in materials science.[1–8] Nowadays, polynuclear Schiff base-metal complexes are attracting a remarkable level of interest.[9,10] Among these materials, the bis-bidentate 4,6-diacetyl resorcinol (DAR) ligand[11] and some DAR-based complexes, such as dioxido and oxidomethoxido vanadium(V), have been synthesized and their catalytic activities investigated.[12,13]

Heterogeneous catalysts have emerged as a possible way of overcoming homogeneous catalysts disadvantages.[14,15] They were prepared by immobilizing the homogeneous catalysts on the surface of solid carriers.[16–21] Among the supports, silica-coated magnetic nanoparticles with thermal stability, simple synthesis and functionalization, easily retrievable with a magnet, and with low toxicity and cost have attracted much attention.[22–27]

One of the most catalytic oxidation reactions is alkane strong C–H-bond oxidation.[28–33] Similar to alkanes, alkenes are some of the most important starting materials for the synthesis of their corresponding carbonyl or carboxylic compounds to epoxides, alcohols, aldehydes, ketones and carboxylic acids[34–38] with many applications in agriculture and industry.[39–42]

Among these carbonyl compounds, adipic acid is a key intermediate in the production of nylon-6,6.[43] The production of this class of organic compounds involves efficient C=C bond oxidation using stoichiometric oxidants such as O_3, $KMnO_4$, RuO_2 and OsO_4 or second- or third-row transition-metal salts or complexes with $NaIO_4$, TBHP and H_2O_2 as the oxidant.[44–46]

Benzoxazole synthetic reactions (Scheme 1),[47] another challenging organic transformation, have generally advanced well, but they are dependent on the consumption of highly poisonous, expensive, corrosive reagents and solvents, non-recyclable catalysts and harsh reaction conditions. These difficulties led to an improvement of catalytic systems, with economical and time-saving one-pot procedures making use of easily available, low-cost materials under mild conditions.[48–50]

[a]*Department of Chemistry, College of Sciences, Shiraz University, Shiraz, 71454, Iran. E-mail: e.safaei@shirazu.ac.ir*

[b]*Department for Synthesis of Materials, Jožef Stefan Institute, Jamova cesta 39, 1000 Ljubljana, Slovenia*

† Electronic supplementary information (ESI) available. See DOI: https://doi.org/10.1039/d2ra06818d

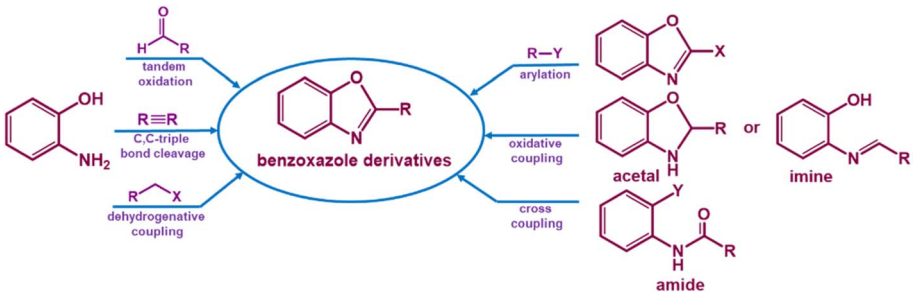

Scheme 1 Some reported procedures for synthesizing a benzoxazole ring.

Benzoxazole derivatives were found to have a vast range of pharmacological and biological actions, and several different synthetic procedures were applied to construct benzoxazole derivatives[51–57] (Scheme 1).

Here, we applied a 4,6-diacyl resorcinol ligand for covalently anchoring on the silica-coated magnetic nanoparticles to design and fabricate a new bimetallic, homogeneously heterogenized catalyst (Scheme 2) to extend green and tolerable nanocatalysts for the above-mentioned challenging organic transformations under mild conditions.

Results and discussion

Synthesis and characterization of Fe_3O_4@SiO_2-APTESFe_2L^{DAR}

Our new, bi-active-site catalyst was synthesized by covalently anchoring the 4,6-diacetyl resorcinol ligand on the silica-coated iron oxide nanoparticles (Fe_3O_4@SiO_2-APTESH_2L^{DAR}), as illustrated by the pathway in Scheme 2. The reaction was followed by the metalation of Fe_3O_4@SiO_2-APTESH_2L^{DAR} by anhydrous $FeCl_3$ (Scheme 2).

Fourier-transform infrared spectroscopy was applied to investigate the covalently grafted ligand and its bimetallic complex on the silica-coated magnetic nanoparticles. The peak at 544 cm^{-1} can be ascribed to the Fe–O stretching vibration, while the peaks at 800–1300 cm^{-1} are the asymmetric and symmetric Si–O–Si and Si–OH stretching. These suggest the presence of a magnetite core and a silica shell on the MNP surfaces of all the particles. In addition, the signals at 2880, 2930 cm^{-1} (symmetric and asymmetric stretching, $-CH_2$ group), 3423 cm^{-1} (stretching vibration, NH bond), and 1480 cm^{-1} (bending vibration, NH_2 and CH_2 groups) confirmed that amino propyl groups were effectively anchored on the silica-coated

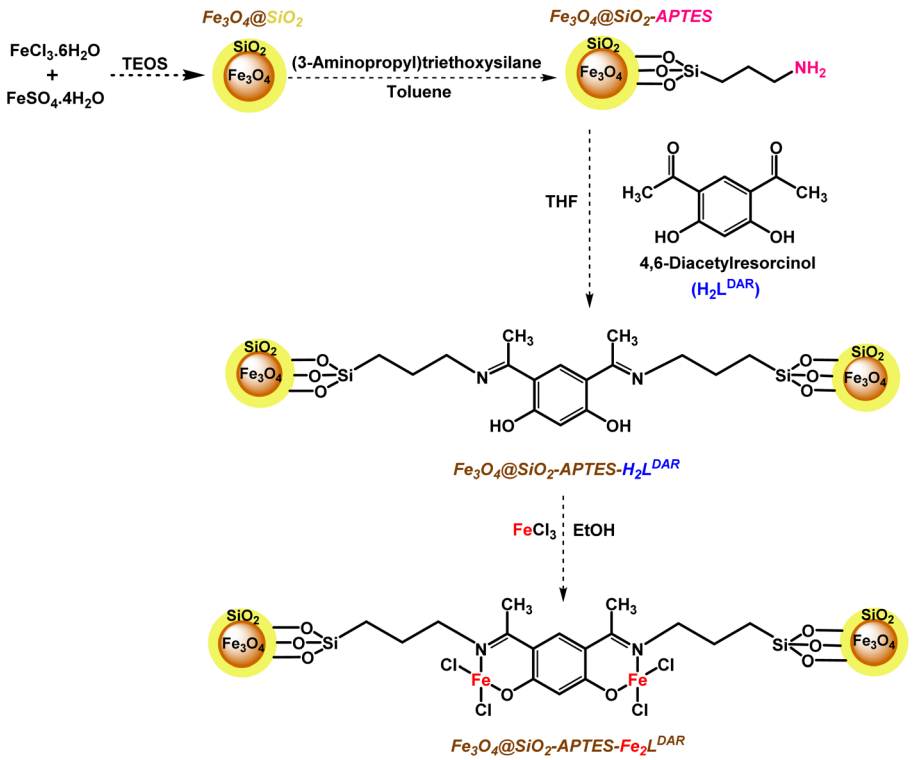

Scheme 2 Schematic synthetic pathway for Fe_3O_4@SiO_2-APTES-Fe_2L^{DAR} catalyst.

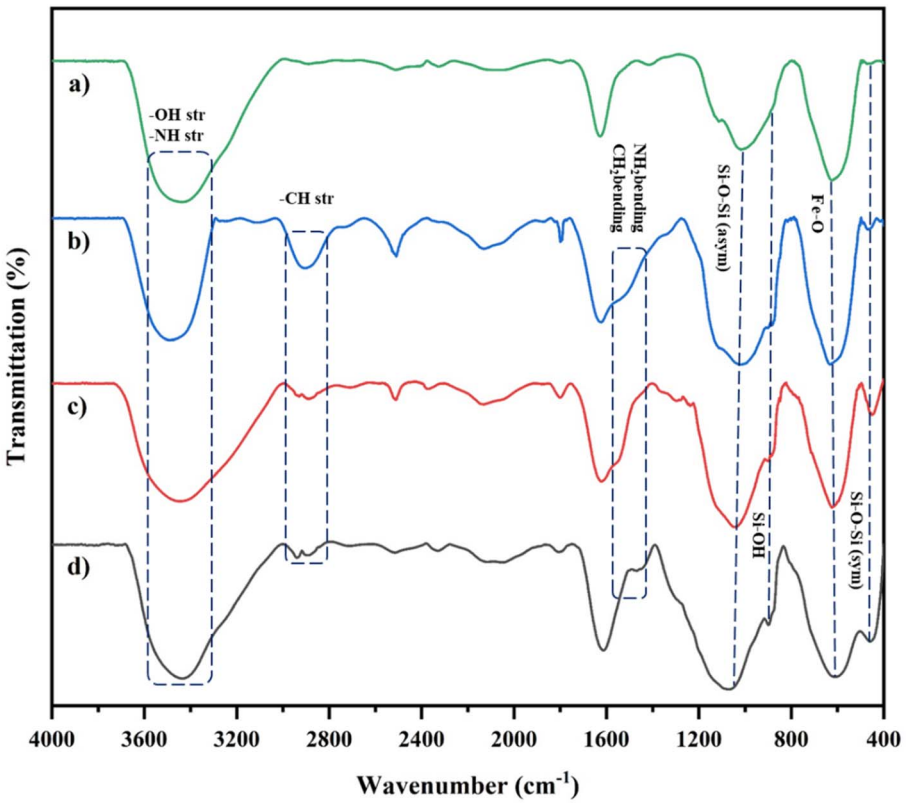

Fig. 1 (a) FTIR spectra of Fe_3O_4@SiO_2; (b) Fe_3O_4@SiO_2-APTES; (c) Fe_3O_4@SiO_2-APTES-H_2L^{DAR}; (d) Fe_3O_4@SiO_2-APTES-Fe_2L^{DAR}.

magnetic nanoparticles. After reacting with the $FeCl_3$ salt, the imine peak emerged at 1620 cm^{-1} by anchoring the ligand on the support, and shifting it to lower frequencies, which confirmed the successful synthesis of the catalyst (Fig. 1).

The morphology, size and structure of the Fe_3O_4@SiO_2-APTESFe_2L^{DAR} were investigated by TEM and FE-SEM. As shown in Fig. 2, this catalyst has a smooth surface with a spherical monotonous morphology. According to the FE-SEM data, the average diameter of the synthesized nanoparticles was less than 40 nm (Fig. 2).

The energy-dispersive X-ray analysis (EDX) revealed the presence of Fe, Si, C, N and O in the final catalyst. In addition, the amount of loading iron on our catalyst was determined by inductively coupled plasma optical emission spectroscopy (ICP-OES) to be 0.3 mmol g^{-1}, which agrees with the EDX result (Fig. S1†). The TEM analysis shows that the iron oxide nanoparticles are well crystallized, and in the range 5–8 nm, coated with a thin, amorphous SiO_2 layer (Fig. 3). The EDXS analysis of the amorphous shell (marked with a white arrow in Fig. 3(b)) showed the presence of Si, O and, to a much lesser extent, of Fe.

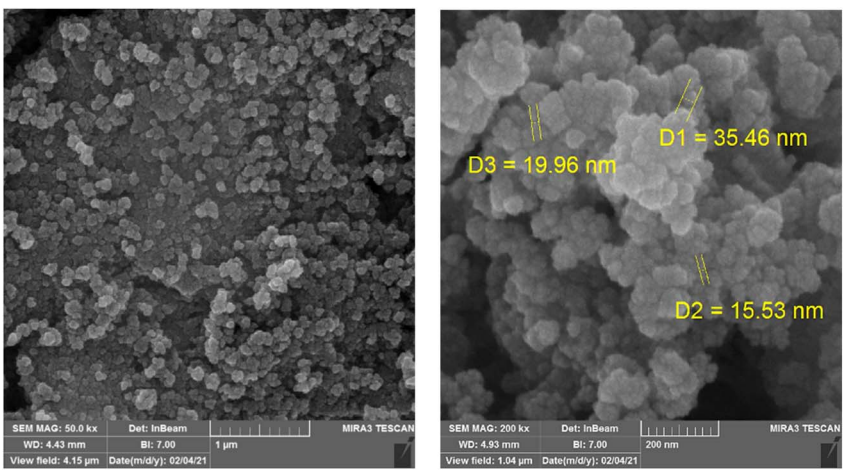

Fig. 2 FE-SEM images Fe_3O_4@SiO_2-APTES-Fe_2L^{DAR} catalyst.

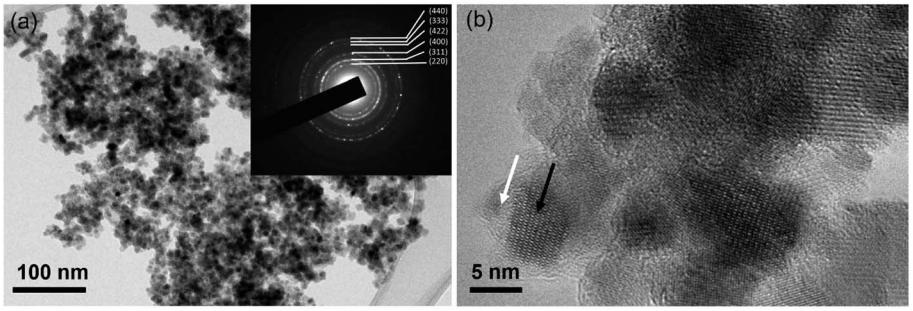

Fig. 3 TEM images of the Fe_3O_4@SiO_2-APTESFe_2L^{DAR} catalysts at lower (a) and higher (b) magnifications. The inset in (a) is a selected-area electron-diffraction pattern acquired from the area indicated in (a) and indexed according to the cubic spinel structure (Space group $Fd\bar{3}m$). The black arrow in (b) shows an iron-oxide nanoparticle, while the white arrow shows an amorphous SiO_2 layer.

In contrast, the analysis in the area indicated by the black arrow (Fig. 3(b)) had a larger content of Fe (in addition to Si and O).

XRD analysis was used to investigate the crystalline structure of the Fe_3O_4@SiO_2-APTESFe_2L^{DAR}. Major characteristic peaks were detected at 30.10°, 35.70°, 43.10°, 53.60°, 57.10° and 62.70° corresponding to the (220), (311), (400), (422), (511) and (440) planes, which indicate a cubic inverse spinel structure without impurity phases (Fig. S2†).

The thermal stability of the magnetic nanoparticles (Fe_3O_4@SiO_2-APTESFe_2L^{DAR}) was examined using TGA. There was a remarkable mass loss in the three steps shown in the TGA curve of the catalyst (Fig. S3†). The mass loss around 200 °C is probably due to the elimination of organic groups of unbounded aminopropyl part of 3-aminopropyltriethoxysilane or DAR covalently bound to it. An additional mass loss from 250 to 520 °C can be attributed to the decomposition of 3-aminopropyltriethoxysilane. The surface of the silica magnetic nanoparticles was coated with 3-aminopropyltriethoxysilane. The decrease in the mass loss at higher temperature demonstrated the anchoring of the ligand on the support and subsequently the metalation of the nanoparticles. The above result confirmed the thermal stability of the catalyst.

The magnetic properties of Fe_3O_4@SiO_2-APTESFe_2L^{DAR} were investigated with a magnetometer. According to Fig. S4,† the hysteresis loop is perfectly reversible, illustrating the superparamagnetic nature of the as-synthesized catalyst. The Fe_3O_4@SiO_2-APTESFe_2L^{DAR} catalyst showed a saturation magnetization value of about 13 emu g^{-1}. As a result, the M_s value of the fabricated catalyst (Fe_3O_4@SiO_2-APTESFe_2L^{DAR}) is sufficient to ensure its facile retrieval from the solution with a magnet.

To determine the presence of all the elements and evaluate of the iron's valence state in the fabricated catalyst, X-ray photoelectron spectroscopy was employed. The binding-energy levels of 56.37, 717.06 and 730.11 eV are ascribed to Fe 3p, Fe $2p_{3/2}$ and Fe $2p_{1/2}$, respectively, which match well with the oxidation states +2 and +3 for the Fe ions. The full-range XPS curve illustrated peaks for C 1s, N 1s, O 1s, Si 2s and Si 2p (Fig. 4). Peaks at 108.58 eV and 160.31 eV were also observed, which confirmed the presence of the silica shell in the catalyst (Fig. S5E and F†). Furthermore, peaks related to O 1s, N 1s and C 1s were found at 538.79, 406.85 and 291.21 eV, which showed the successful attachment of the ligand DAR to the silica-coated MNPs (Fig. S5†).

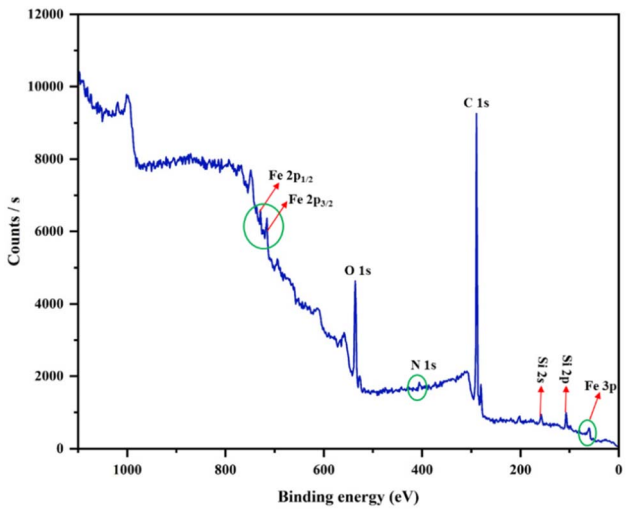

Fig. 4 X-ray photoelectron spectroscopy (XPS) spectrum of catalyst (Fe_3O_4@SiO_2-APTES-Fe_2L^{DAR}).

Catalytic activities

C–H bond oxidation. Some of the main atmospheric contaminants are volatile organic compounds (VOCs), which are found in the atmosphere, deriving from a vast array of gaseous emissions. Catalytic oxidation is a technique for the elimination of VOCs in which contaminants such as the aromatic ring are oxidized completely into the corresponding carbonyl groups, an important precursor for different industries, in the presence of a catalyst.[58,59] Therefore, the activity of the designed catalyst was checked with various reactions. In the beginning, the catalytic efficiency of the designed catalyst (Fe_3O_4@SiO_2-APTESFe_2L^{DAR}) was investigated for the activation of a broad range of alkanes *via* the C–H bond oxidation reaction. To examine the usefulness of the catalyst for this reaction, ethylbenzene was selected as a typical substrate. The ethylbenzene was reacted in the presence of diverse amounts of catalyst, an O_2 balloon as a green oxidant and different reactions times at room temperature. According to Table S1,† H_2O is

Table 1 C–H bond oxidation of diverse alkanes catalyzed by Fe_3O_4@SiO_2APTESFe$_2$L^{DAR}[a]

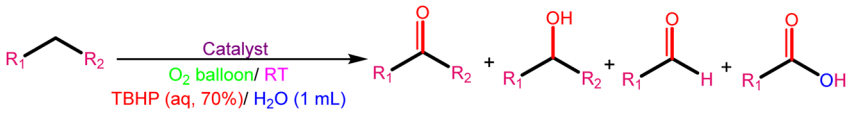

Entry	Substrate	Major product	TBHP[b] (eq.)	Time (h)	Yield[c] (%)	Selectivity[d] (%) to major product	TON[e]
1[f]	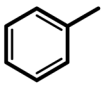	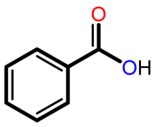	3	20	91	100	75
2[f]	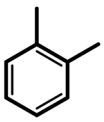	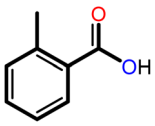	3	20	93	100	77
3[f]	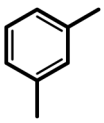	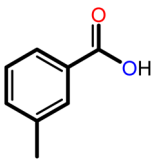	3	20	89	100	74
4[f]	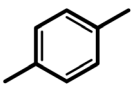	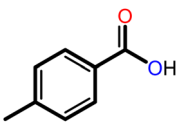	3	20	99	100	82
5[f]	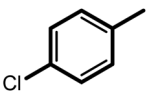	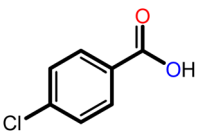	3	20	100	100	83
6[f]	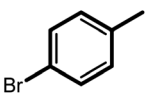	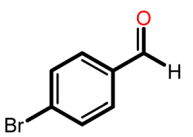	4	20	84	100	70
7[f]	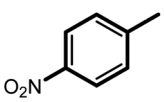	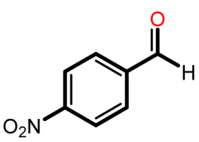	4	20	81	100	67
8[g]	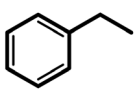	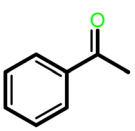	—	15	100	100	111
9[f]	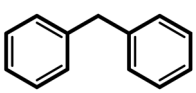	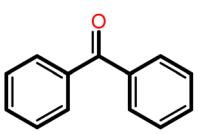	3	20	73	100	61
10[f]	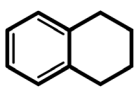	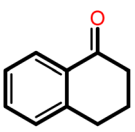	3	22	65	82	54

Table 1 (*Contd.*)

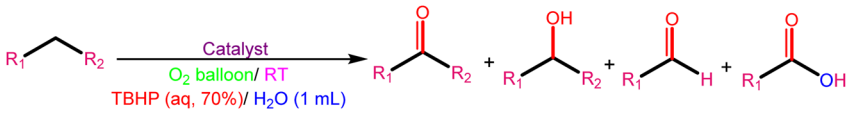

Entry	Substrate	Major product	TBHP[b] (eq.)	Time (h)	Yield[c] (%)	Selectivity[d] (%) to major product	TON[e]
11[f]		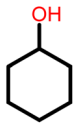	3	22	87	100	72

[a] Reaction conditions: catalyst, substrate (1 mmol), O_2 balloon, H_2O (1 mL), T = room temperature. [b] TBHP (70% in H_2O). [c] Conversions were determined by GC using biphenyl as an internal standard (molar ratio of substrate to internal standard is 1 : 1). [d] Selectivity% = [(product%)/(products%)] × 100. [e] TON = [(moles of alkane converted)/(moles of catalyst)]. [f] 40.0 mg ≈ 1.2 mol%. [g] 30.0 mg ≈ 0.9 mol%.

the best green solvent, due to the harmful effect of VOC-based solvents on the environment. To assess the effect of the amount of catalyst on product yield, the catalytic amount in the reaction was increased from 10.0 mg to 40.0 mg (Table S1,† entries 5–9). The results illustrated that an increment in the amount of the catalyst from 30.0 mg to 40.0 mg does not show any significant change in the product yield. However, the product yield was greatly reduced when the amount of catalyst was reduced to 10.0 mg (Table S1,† entry 9). Therefore, 30.0 mg was the optimized amount of catalyst. To further improve the C–H oxidation reaction, the O_2 balloon was selected as a green oxidant. Consequently, these outcomes strongly proved the excellent performance of the designed catalyst in the aerobic oxidation of ethylbenzene. The catalyst exhibited a high activity for a short time (Table S1,† entry 1) in the presence of the O_2 balloon and TBHP as an oxidant. These results confirm the usefulness of the Fe_3O_4@SiO_2-APTESFe$_2$L^{DAR} catalyst in the presence of each oxidant. Finally, the effect of the reaction time was investigated. An excellent result was achieved in 15 h (Table S1,† entries 2–5). There was almost no outcome when the reaction took place in the presence of the $FeCl_3$ salt as well as with the absence of any catalyst in the blank test (Table S1,† entries 10 and 11). In the following, toluene was selected and reacted in the presence of 2 eq. TBHP and an O_2 balloon with 1 mL H_2O as the solvent, at room temperature (Table S2†). Because the H_2O_2 (being the most common and convenient green oxidant) was degraded by our catalyst, we were obliged to employ *tert*-butyl hydroperoxide (TBHP) as the principal source of oxygen. As Table S2† suggests, in the blank test where there is no catalyst in the system, no conversion was obtained. This proved the role of our catalyst in the C–H bond oxidation (entry 1). Then, the C–H bond's oxidation conditions were optimized by altering the amount of catalyst, the TBHP and the reaction time. According to Table S2† (entry 6), the best result was obtained in the presence of 40.0 mg of catalyst. The toluene conversion is enhanced by increasing the amount of catalyst (Table S2,† entries 3–5). As shown in Table S2† (entries 4 and 6), the toluene conversion when increasing the reaction time to 20 h was nearly completed. The optimal amount of TBHP was 3 eq (Table S2,† entries 2 and 3). The effect of Fe_3O_4@SiO_2-APTES, Fe_3O_4@SiO_2-APTESH$_2$L^{DAR} and Fe_3O_4@SiO_2-APTESFe$_2$L^{DAR} in the presence of the O_2 balloon was compared in the optimized conditions. It can be seen from entries 8 to 10 in Table S2† that the C–H oxidation with two former nanoparticles as a catalyst did not show any favorable selectivity, while the latter led to a carboxylic acid product. Moreover, the performance of the catalyst in the presence of an Ar balloon showed less selectivity, in comparison to the O_2 balloon. We developed an investigation under optimized conditions to cover a range of alkanes to oxidize the C–H bond under aqueous conditions at 25 °C in the presence of TBHP and O_2 as the oxidants (Table 1, entries 1–11). After the C–H bond is broken, it is possible that all the product shown in Table 1 forms in the reaction solution. However, the synthesized catalyst promotes the formation of one of these products selectively, depending on the presence of donating or accepting groups on the substrate.

We studied the rate *vs.* [substrate] monitoring of the C–H activation reactions with various concentrations of the substrate. Fig. 5 shows a linear relationship was obtained for the reaction rate *versus* [S]. Fig. 5 suggests that the reaction

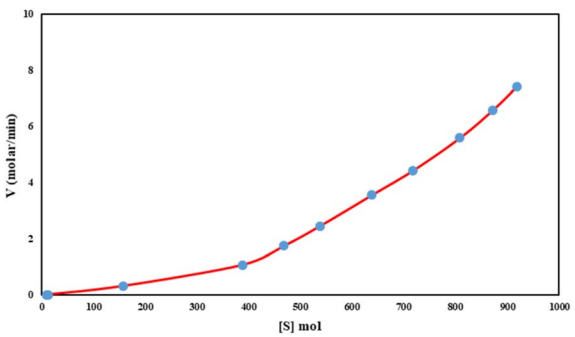

Fig. 5 Rate *vs.* [substrate] monitoring profile of Fe_3O_4@SiO_2-APTES-Fe$_2$L^{DAR}.

includes two steps. In the first step, the rate of reaction is very slow with a small slope ($K = 0.001$) since O_2 as an oxidant reacts with the catalyst to produce a high-valent iron oxo species, which in turn attaches to the substrate with a higher rate ($K = 0.01$).

C=C bond oxidative cleavage. The oxidative cleavage of some alkenes using a bimetallic catalyst has been extensively examined in the literature. First, the oxidative cleavage of 1-hexene as a typical substrate (2 mmol), using O_2 as a green oxidant and Na_2SO_3 as a co-catalyst in the presence of various amounts of the catalyst at ambient temperature, was examined. Of the different amounts of catalyst, 0.050 g had the highest catalytic activity (Table S3,† entry 4). The C=C bond oxidation could not be applied without a solvent (entry 9). The conversion could be increased to 94% using CH_3CN as a green solvent, which is a better conversion result than with the H_2O/acetone mixture (Table S3,† entries 4 and 10). According to Table S3,† different reaction times were also examined. The highest conversion and selectivity were obtained at 15 h (entries 4 and 5). In addition, different amounts of Na_2SO_3 as a co-catalyst were investigated (Table S3,† entries 4, 6 and 7). The conversion increased from 67% to 94% in the presence of 2 mmol Na_2SO_3. In the blank test, where there is no catalyst, and in the presence of $FeCl_3$ under the reaction conditions there was no

Table 2 Oxidative cleavage of diverse alkenes catalyzed by Fe_3O_4@SiO_2APTESFe_2L^{DAR}[a]

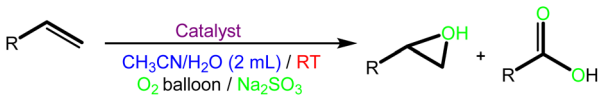

Entry	Substrate	Major product	Time (h)	Yield[b] (%)	Selectivity[c] (%) to major product	TON[d]
1	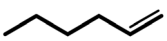	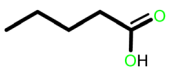	15	94	100	62
2		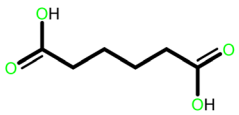	24	87	100	58
3	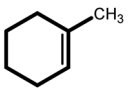	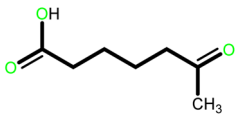	24	82	100	54
4	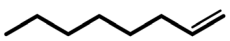	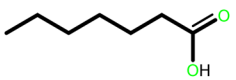	15	92	100	61
5	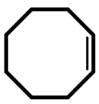	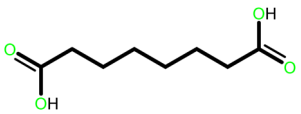	20	90	100	60
6	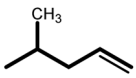	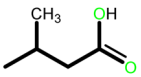	18	90	100	60
7	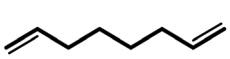	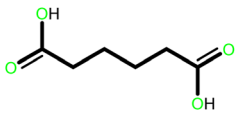	24	91	100	60
8	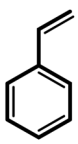	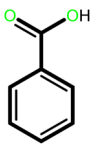	24	92	100	61
9	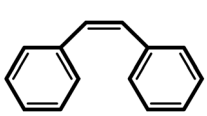	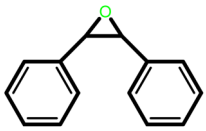	24	93	100	62

[a] Reaction conditions: catalyst (50.0 mg, 1.5 mol%), substrate (2 mmol), O_2 balloon, H_2O/CH_3CN (2 mL), Na_2SO_3 (2 mmol, 0.24 g), T = room temperature. [b] Isolated yield. [c] Selectivity% = [(product%)/(products%)] × 100. [d] TON = [(moles of alkene converted)/(moles of catalyst)].

oxidative cleavage of 1-hexene (Table S3,† entry 1 and 14). Also, other nanoparticles such as Fe_3O_4@SiO_2-APTES, Fe_3O_4@SiO_2-APTESH_2L^{DAR} under the reaction conditions were much less effective for the C=C bond oxidation than the Fe_3O_4@SiO_2-APTESFe_2L^{DAR} (Table S3,† entries 11–13). Afterwards, the C=C bond oxidation of cyclohexene was examined. This reaction proceeded to result in carbonyl-containing compounds (Table S4†). The use of 0.050 g of catalyst at RT led to the highest activity of cyclohexene to adipic acid with O_2 as the oxidant and Na_2SO_3 as the co-catalyst (Table S4,† entries 2–4). Cyclohexene can be transformed into 87% adipic acid in CH_3CN as the best solvent (Table S4,† entries 4 and 8). According to Table S4,† in solvent-free conditions cyclohexene cannot be converted to adipic acid (Table S4,† entries 9–11). As shown in Table S4† (entry 4), 2 mmol of Na_2SO_3 increased the conversion of adipic acid up to 87% after 24 h. Therefore, the Fe_3O_4@SiO_2-APTESFe_2L^{DAR} catalyst can cleave cyclohexene to adipic acid using 0.050 g of catalyst, CH_3CN, 2 mmol Na_2SO_3 in the presence of O_2 as oxidant at RT (Table S4,† entry 4). Furthermore, the Fe_3O_4@SiO_2-APTESFe_2L^{DAR} catalyst was applicable to the C=C bond oxidation of diverse alkenes under these conditions (Table 2). It is worth noting that both epoxide and acid products can be produced after breaking the C=C bond in the reaction solution. However, one of these products forms in larger amounts due to the selective performance of the catalyst. The nature of the alkenes is significant in the conversion of the products. Linear terminal alkenes show a remarkably higher activity in this oxidative cleavage than the cyclic alkenes.

Benzoxazoles synthesis. Compared to Scheme 1, the benzoxazole synthesis proceeds through the reaction of 3,5-di-*tert*-butylbenzene-1,2-diol (0.5 mmol), 4-bromobenzaldehyde (0.5 mmol) and NH_4OAc as the nitrogen resource, green solvent in the reaction. Initially, H_2O was chosen as the green solvent in the solvent-free conditions at RT (Table S5,† entries 1 and 2). The effect of temperature on the aqueous media reaction was investigated and the conversion yield was low at RT (Table S5,† entries 3 and 4). After increasing the temperature to 70 °C for 10 h, 97% of the product was obtained (entry 4). Decreasing the reaction time to 7 h led to a lower conversion percentage (Table S5,† entry 6). To investigate a suitable amount of catalyst, 30.0, 40.0 and 50.0 mg of catalyst were tested. Using 40.0 mg of the catalyst in this reaction, an excellent yield of the product was obtained (Table S5,† entry 5). Moreover, the amount of NH_4OAc (as a nitrogen source) was also investigated. The optimized amount of NH_4OAc was 0.5 mmol (Table S5,† entries 10 and 11). To examine the efficacy of Fe_3O_4@SiO_2-APTESFe_2L^{DAR} on the catalytic activity of benzoxazole preparation, reference tests were performed. The results show that the nanoparticles and $FeCl_3$ have negligible catalytic activity in the synthesis of benzoxazoles (Table S5,† entries 12–14). As shown in Table S5,† the best outcome for the synthesis of product 3a from 3,5-di-*tert*-butylbenzene-1,2-diol (0.5 mmol), NH_4OAc (0.5 mmol) as a nitrogen resource and 4-bromobenzaldehyde (0.5 mmol) were acquired in H_2O at 70 °C in the presence of Fe_3O_4@SiO_2-APTESFe_2L^{DAR} as a catalyst. We screened this procedure of benzoxazole synthesis by reversing the aryl aldehydes with

Table 3 Reaction of various aldehydes under optimization conditions catalyzed by Fe_3O_4@SiO_2-APTES-Fe_2L^{DAR}[a]

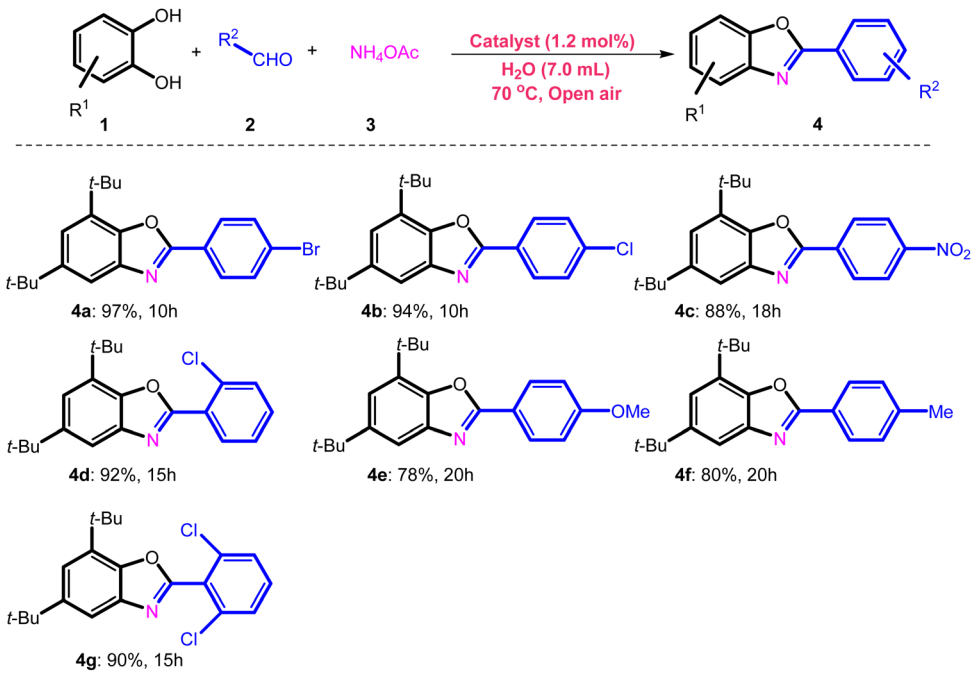

[a] Reaction conditions: Fe_3O_4@SiO_2-APTES-Fe_2L^{DAR} (40.0 mg, 1.2 mol%), 3,5-di-*tert*-butylbenzene-1,2-diol (0.5 mmol), NH_4OAc (0.5 mmol) and aldehyde (0.5 mmol), H_2O (7 mL), 70 °C and reflux.

various electron-accepting and electron-donating groups under the optimized conditions. As illustrated in Table 3, the aryl aldehydes consisting of electron-accepting groups at the *para* and *ortho* positions led to excellent yields of benzoxazoles. Aryl aldehydes with methyl and methoxy groups (electron-donating groups) at the *para* position were obtained with 80% and 78% yields, respectively (Table 3, entries 6 and 7). All the benzoxazoles derivatives were characterized using ^{1}H NMR.

Recyclability of the catalyst and the hot-filtration test

Among the diverse properties of a catalyst, recyclability is the most fundamental one as this relates to the performance and economics of a process from the industrial viewpoint. So, to prove the recyclability of our catalyst, after each cycle the catalyst was collected from the solution using a magnet, rinsed with acetone and dried under vacuum. Fig. 6a shows that the catalyst was used for eight consecutive runs without a tangible decline in the product yield. In addition, to examine the possibility of leaching the catalyst, Sheldon's hot-filtration test was applied for the C–H bond oxidation reaction under optimized conditions. During the C–H bond oxidation reaction of ethylbenzene, the catalyst was magnetically eliminated from the solution after 7.5 h. After this the reaction was continued without the catalyst for 7.5 h (Table 4). Finally, the reaction was stopped and monitored by GC to characterize the product yield, which rejected leaching and proved that the catalyst proceeded the reaction pathway. After completing the C=C bond oxidation of 1-hexene under these conditions, the Fe_3O_4@SiO_2-APTESFe_2L^{DAR} catalyst could be easily retrieved from the solution with a magnet. No significant leaching of the Fe ions was observed using atomic absorption spectroscopy (AAS). Also, the retrieved Fe_3O_4@SiO_2-

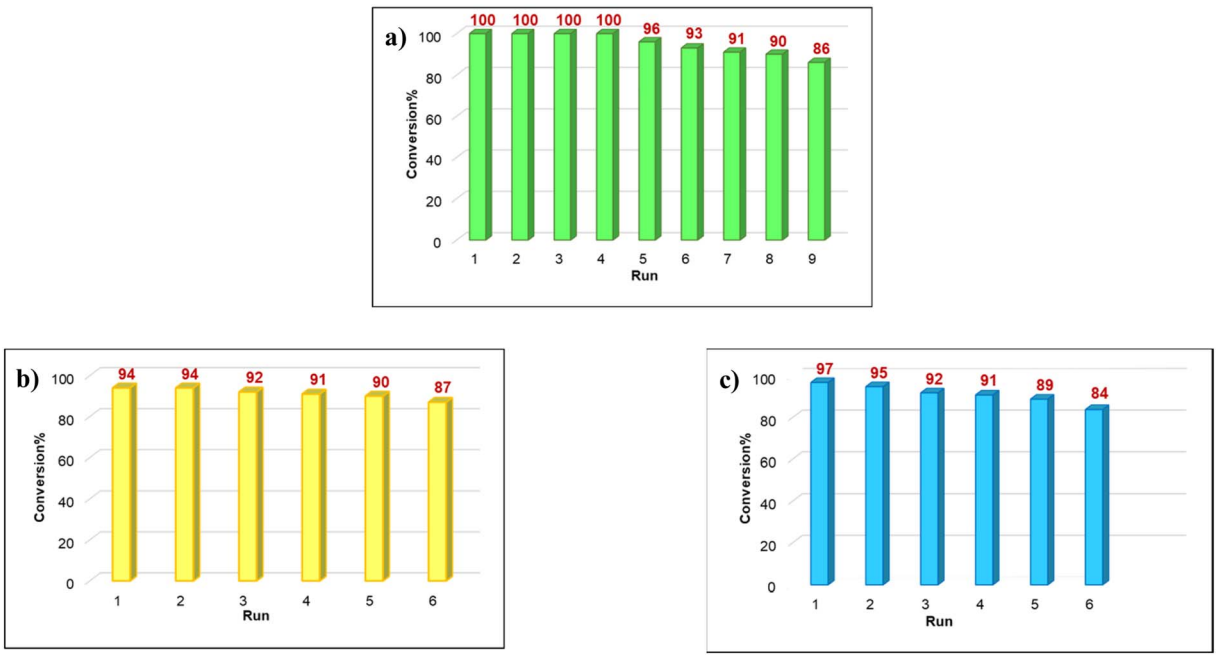

Fig. 6 (a) Recycling of catalyst in the oxidation of alkanes; (b) oxidative cleavage of alkenes; (c) reaction synthesis of benzoxazoles.

Table 4 Sheldon's hot-filtration test for the C–H bond's oxidation of ethylbenzene[a]

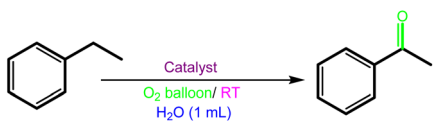

Entry	Catalyst type	Catalyst amount (mg)	Time[b] (h)	Temp. (°C)	Conv.[c] (%)
1	Fe_3O_4@SiO_2APTESFe_2L^{DAR}	30.0	7.5 (before filtering)	25	27
2	Fe_3O_4@SiO_2APTESFe_2L^{DAR}	30.0	7.5 (after filtering)	25	34
3	Fe_3O_4@SiO_2APTESFe_2L^{DAR}	30.0	15	25	100

[a] Reaction conditions: catalyst (30.0 mg ≈ 0.9 mol%), substrate (1 mmol), O_2 balloon, H_2O (1 mL), T = room temperature. [b] Hot filtration test. [c] Conversions were determined by GC using biphenyl as an internal standard (molar ratio of substrate to internal standard is 1 : 1).

$APTESFe_2L^{DAR}$ catalyst without a considerable change in the conversion and selectivity could be reused for a fifth run (Fig. 6c). Furthermore, for the benzoxazole synthesis 3,5-di-*tert*-butylbenzene-1,2-diol (0.5 mmol), 4-bromobenzaldehyde (0.5 mmol) and NH_4OAc (0.5 mmol), the data obtained using atomic absorption spectroscopy (AAS) confirmed that the leached amount of Fe after the completion of the reaction was very low and that the nature of the catalyst for these reactions is heterogeneous. It is noteworthy that the retrieved $Fe_3O_4@SiO_2$-$APTESFe_2L^{DAR}$ catalyst had a comparable activity even after the fifth run in the benzoxazoles synthesis (Fig. 6b).

The C–H/C=C bond oxidation reactions and the benzoxazoles synthesis using heterogeneous bimetallic catalysts under mild conditions are rare. Therefore, we compared our outcomes with some other catalyst systems (Table 5). This showed that $Fe_3O_4@SiO_2$-$APTESFe_2L^{DAR}$ has excellent applicability in both the C–H/C=C bond oxidation reactions and the synthesis of benzoxazoles.

Table 5 Efficiency comparison of the $Fe_3O_4@SiO_2$-APTES-Fe_2L^{DAR} catalyst with diverse catalysts in some recent publications

Entry	Catalyst	Reaction conditions	Conv. (%)	Major product
C–H bond oxygenation				
1 (ref. 60)	Fe_3O_4MNPs (10 mol%)	Ethylbenzene (1 mmol), TBHP (70% aq., 0.5 mmol), $T = 120$ °C, time = 3 h	93	Acetophenone
2 (ref. 61)	HKUST-1@Cu–$CuFe_2O_4$ (15.0 mg)	Ethylbenzene (1 mmol), CH_3CN (5 mL), *N*-hydroxyphthalimide (10 mol%), $T = 60$ °C, 1 atm O_2, time = 9 h	93	Acetophenone
3 (ref. 62)	$Mn(OH)_x/\gamma$-Al_2O_3 (0.03 mmol)	Ethylbenzene (40 mmol), O_2 flow (5 mL min^{-1}), benzoic acid (0.4 mmol), $T = 135$ °C, time = 24 h	74	Acetophenone
4 (ref. 63)	$FeVO_4$/g-C_3N_4 (50.0 mg) nanocomposites	Ethylbenzene (10 mmol), CH_3CN (6 mL), H_2O_2 (25 mmol), $T = 60$ °C time = 4 h	91	Acetophenone
5 (ref. 64)	Mn–N–C@SiO_2, (30 mg)	Ethylbenzene (10 mL), O_2 (0.8 MPa), $T = 120$ °C time = 5 h	12	Acetophenone
6 (ref. 65)	Ruthenium complex (0.004 mmol)	Ethylbenzene (4 mmol), TBHP (12 mmol), $T = 40$ °C time = 26 h	82	Acetophenone
7 (ref. 66)	Mn@SiO_2/Al_2O_3, mixed oxide (50.0 mg)	Ethylbenzene (1.14 mL, 2 mmol), TBHP 80% (1.34 mL, 2 mmol), $T = 80$ °C time = 24 h	67	Acetophenone
8 this work	$Fe_3O_4@SiO_2$-APTES-Fe_2L^{DAR} (30.0 mg, 0.9 mol%)	Ethylbenzene (1 mmol), H_2O (1 mL), RT, time = 15 h, O_2	100	Acetophenone
C=C bond oxidative cleavage				
9 (ref. 67)	$SiRu(H_2O)W_{11}O_{39}$ $((C_6H_{13})_4N)_5$ (0.2 mol%)	Cyclohexene (1 mmol), 5 equiv. $KHSO_5$, 1,2-dichloroethane/H_2O 1 : 1, time = 4 h, $T = 60$ °C	67	Adipic acid
10 (ref. 68)	$WO(O_2)_2L_2^{2-}$ (L = oxalic acid), (1 mol%)	Cyclohexene (0.3 mmol), 30% H_2O_2 (134 mL), time = 24 h, $T = 94$ °C	96	Adipic acid
11 (ref. 69)	Cu-salen-PPh_3, (8 mmol)	Cyclohexene (1 mmol), 2.6 equiv. 30% H_2O_2, H_3PO_4, [Emim]PF_6 CH_2Cl_2 (1 : 1), time = 3 h	96	Cyclohexen oxide
12 (ref. 70)	C-PMA_n-V, (27–38 wt%) (30.0 mg)	Cyclohexene (1 mmol), 8 equiv. TBHP, H_2O, time = 32 h, $T = 105$ °C	67	Adipic acid
13 (ref. 71)	POM on oxide supports (50 wt%)	Cyclohexene (1 mmol), 3–4 equiv. 30% H_2O_2, 2-methylpropan-2-ol, time = 24 h, $T = 60$ °C	90	Adipic acid
14 (ref. 72)	Ru on charcoal, (1 mol%)	Cyclohexene (1 mmol), 1.1 equiv. $NaIO_4$, MeCN : EtOAc : H_2O 1 : 1 : 1 (v/v), time = 7.5 h	42	Adipic acid
15 this work	$Fe_3O_4@SiO_2$-APTES-Fe_2L^{DAR} (50.0 mg, 1.5 mol%)	Cyclohexene (2 mmol), H_2O (2 mL), $NaSO_3$ (2 mmol), RT, time = 24 h, O_2	87	Adipic acid
Benzoxazole synthesis				
16 (ref. 73)	$(FeL^{APIP})_2O$ (1.2 mol%)	Bromo aminophenol (1 mmol), TBHP (70%, 0.4 mL), H_2O (5 mL), time = 8 h	83	4,6-Di-*tert*-butyl-2-(4-boromophenyl)-1*H*-benzo[*d*]oxazole
17 (ref. 74)	Fe(III)-salen (3 mol%)	3-Bromobenzaldehyde (1 mmol), EtOH (5 mL), $T = 50$ °C, time = 5 h	80	4,6-Di-*tert*-butyl-2-(3-boromophenyl)-1*H*-benzo[*d*]oxazole
18 (ref. 75)	$RuCl_3$	4-Bromobenzaldehyde (1 mmol), [bmim]BF_4 1 mL, $T = 80$ °C, time = 10 h	78	4,6-Di-*tert*-butyl-2-(4-boromophenyl)-1*H*-benzo[*d*]oxazole
19 this work	$Fe_3O_4@SiO_2$-APTES-Fe_2L^{DAR} (40.0 mg, 1.2 mol%)	4-Bromobenzaldehyde (1 mmol), H_2O (7 mL), $T = 70$ °C, time = 10 h	97	4,6-Di-*tert*-butyl-2-(4-boromophenyl)-1*H*-benzo[*d*]oxazole

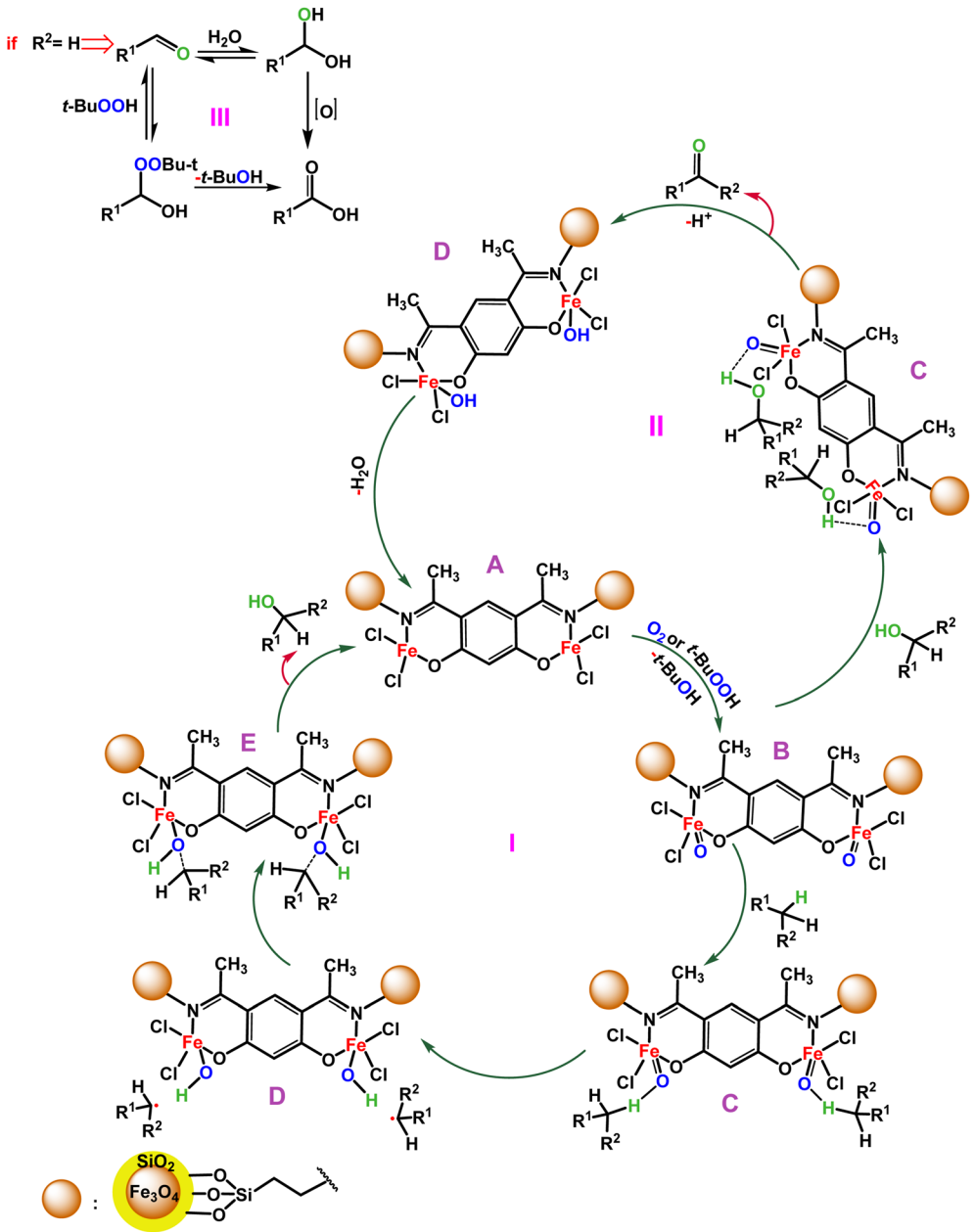

Scheme 3 Proposed mechanism for C–H bond oxygenation of the Fe_3O_4@SiO_2-APTES-Fe_2L^{DAR} catalyst to different products (I) alcohol, (II) ketone, (III) acid.

Proposed mechanisms

Proposed mechanisms for C–H bond oxidation. As illustrated in Scheme 3, we propose a mechanism for the C–H bond oxidation by the Fe_3O_4@SiO_2-APTESFe_2L^{DAR} catalyst. The catalytic cycle begins in the presence of the bimetallic complex and TBHP and/or O_2, which oxidize the iron(III) complex to produce high-valent metal-oxo species by binding to the iron(III) in the catalyst's structure.[76,77] This species in turn produces short-lived alkyl radicals in the C–H bond's oxidation (cycle I). In view of the products obtained from the C–H bond oxidation, the alcohol produced transforms to its corresponding aldehyde or ketone (cycle II). With further oxidation of the resulting benzaldehydes using more oxidant, a benzoic acid product is obtained (cycle III).[78,79]

Proposed mechanisms for C=C bond oxidative cleavage. The possible oxidation mechanism of the C=C bond in the presence of the Fe_3O_4@SiO_2-APTES-Fe_2L^{DAR} catalyst involves forming a high-valent iron-oxo species too. According to Scheme 4, SO_3^{2-} reduces the Fe(III) to Fe(II), which is very stimulated to react with the alkene. In the following, we postulate that the oxidation proceeds by an initial coordination

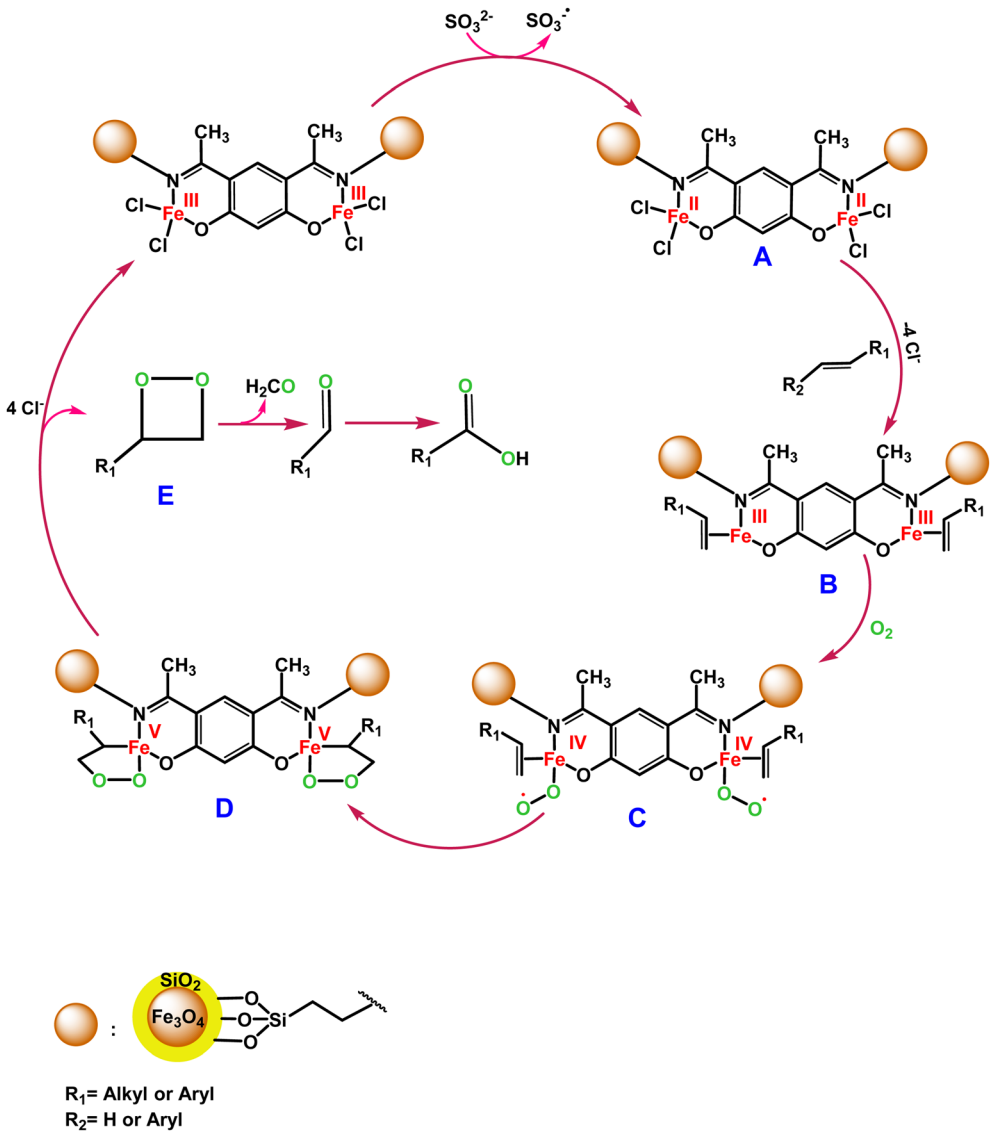

Scheme 4 Proposed mechanism for C=C bond oxidative cleavage of the Fe_3O_4@SiO_2-APTES-Fe_2L^{DAR} catalyst.

of alkene to the Fe(II) centre of the Fe_3O_4@SiO_2-APTESFe_2L^{DAR} catalyst (B). Then the reaction is followed by an interaction with molecular O_2 to produce the superoxo radical (C). Afterwards, the intermediate (C) undergoes cyclization with the alkene (D). Then dioxetane (E) was produced during the resulting peroxo metallacycle decomposition. It disintegrated to produce the benzaldehyde,[80] the further oxidation of which produces benzoic acid (Scheme 4).

Proposed mechanisms for benzoxazole synthesis. According to the results acquired in the synthesis of benzoxazoles from the reaction of 3,5-di-*tert*-butylbenzene-1,2-diol, NH_4OAc and various benzaldehydes by Fe_3O_4@SiO_2-APTESFe_2L^{DAR} catalyst, we propose a mechanism based on previous research,[74] which is illustrated in Scheme 5. To start, catechol was coordinated to the catalyst, which resulted in the production of its corresponding one- and two-electron oxidized products of semiquinone and quinone, respectively. The colour change of the mixture to green is a proof of the catechol oxidation process. The UV-vis spectrum of the reaction mixture shows the absorption bond related to quinone (Fig. S6†). Meanwhile, the ammonia produced from the dissociating ammonium acetate reacted with the aldehyde and oxidized the 3,5-di-*tert*-butylbenzene-1,2-diol, using the nucleophilic attack of phenyl methane imine intermediate II, which is converted to the intermediate III.[81] Then, the hydroxyl radical of the intermediate III was eliminated and produced the imine intermediate IV. The phenoxyl radical intermediate V was generated using a single-electron transfer (SET) of imine intermediate IV and the hydroxyl radical.[82] At the end of mechanism, through SET and intramolecular cyclization of intermediate V created the

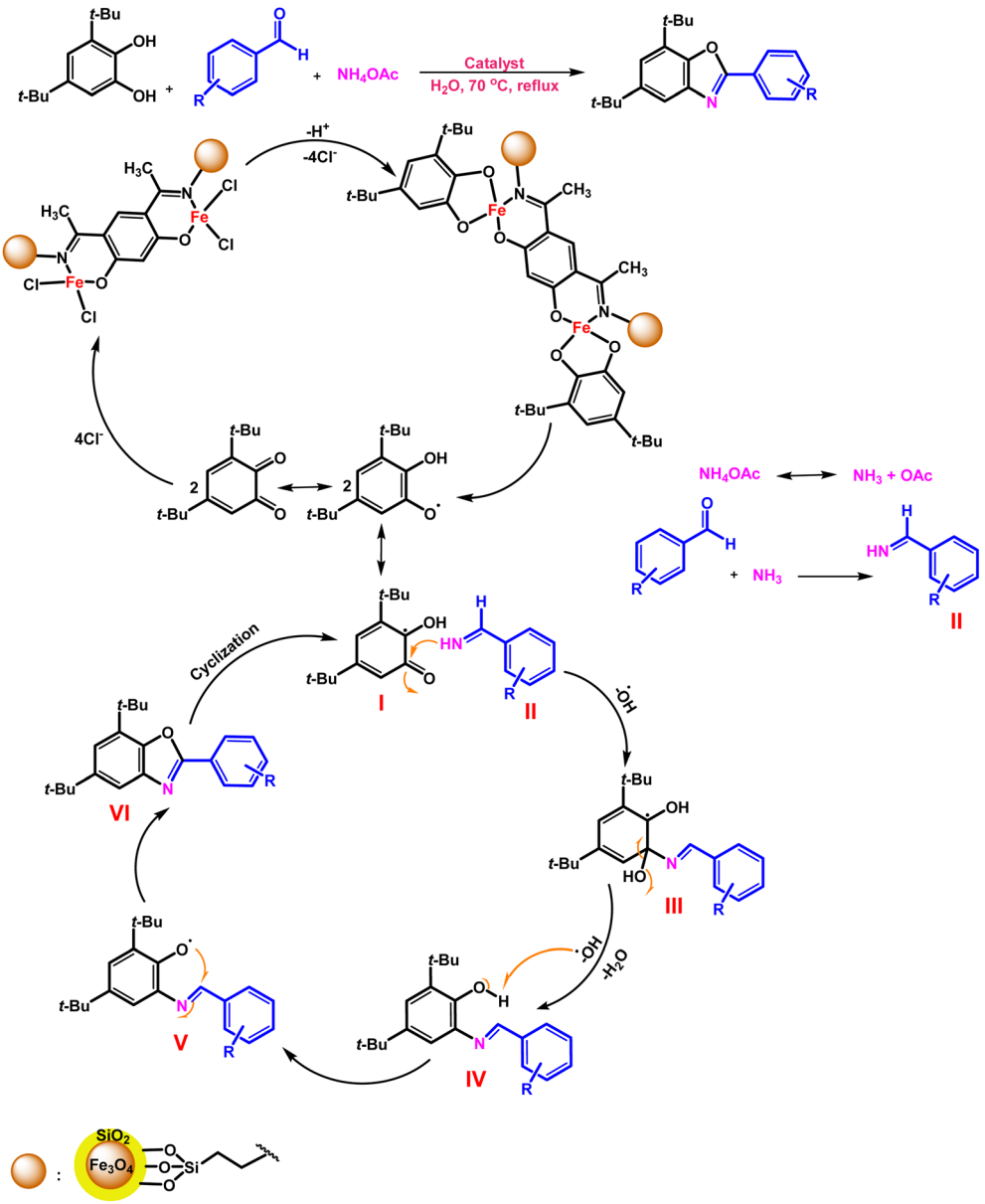

Scheme 5 Proposed mechanism for benzoxazoles synthesis reaction of the Fe_3O_4@SiO_2-APTES-Fe_2L^{DAR} catalyst.

favorable benzoxazoles VI (Scheme 5).[83] Inasmuch as no consequence was found when the reaction occurred in the presence of TEMPO (2,2,6,6-tetramethyl piperidin-1-yl)oxyl, it confirmed the proposed radical mechanism.

Conclusion

For the first time the synthesis and characterization of a homogeneously heterogenized binuclear iron(III) complex of covalently anchored 4,6-diacetyl resorcinol on silica-coated magnetic nanoparticles (Fe_3O_4@SiO_2-APTESFe_2L^{DAR}) is reported. Moreover, the catalytic application of this catalyst for C–H and C=C bond oxidation of a wide range of alkanes and alkenes was investigated. In addition, a one-pot multicomponent reaction for the synthesis of benzoxazole derivatives from 3,5-di-*tert*-butylbenzene-1,2-diol, diverse aldehydes and ammonium acetate as the nitrogen source was performed. The as-synthesized bimetallic (or better as the bi-active catalyst) displays remarkable catalytic activities under mild reaction conditions and in water. Based on our knowledge, the C–H oxidation of alkanes is mostly performed under the harsh reactions of high temperature and organic solvents, and iron complexes usually do not show good reactivity for this class of organic reactions unless harsh conditions are applied. Furthermore, excellent conversion and selectivity in C=C bond oxidation is observed with the addition of an appropriate amount of Na_2SO_3 as the co-catalyst in comparison to the mentioned bimetallic catalyst. An analysis of the products shows that except in one case, some oxidative cleavages of the cyclic and terminal alkenes was observed. Among them, producing adipic acid and some other bifunctional

carboxylic acids are important in terms of polymerization. Importantly, the recyclability and reusability of this bimetallic catalyst remained after the eighth, fifth and fifth consecutive runs for C–H, C=C bond oxidation and in the benzoxazole synthesis, respectively, without any tangible loss in catalytic activities. Moreover, the leaching tests in the C–H/C=C bond oxidation and the benzoxazole synthesis process confirmed that the binuclear complex was immobilized tightly to the magnetite nanoparticles and the reactions proceed *via* a heterogeneous pathway. The designing of a bi-ferric catalyst and the dramatic effect of having two active sites in one structure on the catalyst function makes this a credible candidate for green chemistry.

Experimental

Materials and methods

All chemical reagents and solvents were supplied by Acros Organics, Sigma Aldrich, Fluka and Merck and used as received. The FT-IR spectra of nanoparticles were recorded in the range 400–4000 cm^{-1} in the solid state on a Shimadzu FT-IR 8300 spectrophotometer. Scanning electron microscopy (SEM) (JEOL, JSM-5600) was used to observe the morphology of the catalyst. Iron oxide nanoparticles and silica coating were observed by transmission electron microscopy (TEM) (JEOL JEM 2100), while elemental composition was determined using energy-dispersive X-ray spectroscopy (EDXS) (JEOL Jed 2300). The X-ray diffraction (XRD) pattern was captured by a PHILLIPS PW1730 (using step size of 0.05 and time per step of 1 s). Using a PerkinElmer 240-B microanalyzer, the elemental analysis (C, H and N) was accomplished. The hysteresis curve was measured with a vibrating-sample magnetometer at RT from −15000 to +15000 Oe. Thermal gravimetric analyses (TGA) were recorded under nitrogen on Netzsch STA 409 PC/PG instrument with a heating rate of 20 °C min^{-1} up to 800 °C. To measure the electronic state of the catalyst elements, an XPS multilab 2000 with Al-Kα radiation was used. The EDX analysis was obtained with a Tescan Mira (II) at an acceleration voltage of 15 kV. The content of Fe in the catalyst was calculated using an inductively coupled plasma-optical emission spectrometer (ICP-OES). The mixture reactions were monitored by thin-layer chromatography (TLC) and gas chromatography (GC, Agilent gas chromatograph model 7890 A) using a flame-ionization detector. The ^{1}H NMR spectra were recorded with a 250 MHz Bruker Avance instrument in $CDCl_3$ or DMSO-d_6 as solvents and tetramethyl silane (TMS) as internal standard.

Synthesis of Fe_3O_4@SiO_2-APTES

The magnetic Fe_3O_4 MNPs, silica-coated nanoparticles (Fe_3O_4-$\cdot SiO_2$) and the functionalized (Fe_3O_4@SiO_2-APTES) form were acquired *via* the reported method.[84]

Synthesis of 4,6-diacetylresorcinol covalently anchored on nanomagnet (Fe_3O_4@SiO_2-APTESH_2L^{DAR}) and its iron(III) complex (Fe_3O_4@SiO_2-APTESFe_2L^{DAR})

Fe_3O_4@SiO_2-APTESH_2L^{DAR} was prepared by adding 4,6-diacetylresorcinol (4.37 mmol, 0.85 g) to a suspension containing Fe_3O_4@SiO_2-APTES and dry THF (25 mL) with vigorous stirring for 4 days at room temperature. Afterwards the solid product was gathered with a magnet and rinsed with ethanol, CH_2Cl_2, acetone and dried under vacuum at 70 °C for 24 h.

The modified MNPs (Fe_3O_4@SiO_2-APTES-H_2L^{DAR}) were scattered in absolute ethanol (20 mL), then triethyl amine (0.5 mmol, 0.050 g) was slowly added to the solution after 45 min stirring at room temperature, $FeCl_3$ (0.5 mmol, 0.082 g) was added to the resulting mixture, then was again stirred for 4 days at room temperature. Finally, the brown product was gathered using a magnetic field and rinsed with EtOH, CH_2Cl_2, acetone and dried in a vacuum oven at 80 °C for 24 hours (Fe_3O_4@SiO_2-APTESFe_2L^{DAR}).

The C–H bond oxidation procedure

To a 10 mL flask containing a mixture of H_2O (1 mL, saturated with O_2 for 15 minutes), TBHP (2–4 eq) as the oxidant and substrate (1 mmol), Fe_3O_4@SiO_2-APTESFe_2L^{DAR} (0.040 g, 1.2 mol%) was added and the mixture was stirred in the presence of O_2 (from a balloon) at RT. The reaction's progress was followed by TLC. At the end, the mixture was elicited with ethyl acetate then the catalyst recycled with a magnetic field. Finally, the products were characterized *via* gas chromatography and ^{1}H NMR spectroscopy.

The C=C bond oxidative cleavage procedure

To a 10 mL flask containing a mixture of CH_3CN (2 mL, saturated with O_2 for 15 minutes), Na_2SO_3 (2 mmol) as the co-catalyst and substrate (2 mmol) was added Fe_3O_4@SiO_2-APTESFe_2L^{DAR} (0.050 g, 1.5 mol%) and the mixture was stirred in the presence of O_2 (from a balloon) at RT. Finally, the aforementioned mixture was elicited with ethyl acetate and the catalyst recycled with a magnetic field. At the end, the products were characterized by ^{1}H NMR spectroscopy.

The synthesis of benzoxazoles procedure

3,5-di-*tert*-butylbenzene-1,2-diol (0.5 mmol), aldehyde (0.5 mmol), NH_4OAc (0.5 mmol, 0.05 g) in H_2O (7 mL) and catalyst (0.040 g, 1.2 mol%) were added to a 15 mL round-bottom flask. Then, the mixture was stirred at 70 °C magnetically under refluxing. The reaction's progress was followed by TLC. Finally, the mixture was elicited with ethyl acetate then the catalyst recycled using a magnetic field. Utilizing a mixture of *n*-hexane/EtOAc as an eluent, the residue was purified by column chromatography on silica to arrive at the pure product. Finally, the products were characterized by ^{1}H NMR spectroscopy.

Conflicts of interest

There is no conflict of interest to declare.

Acknowledgements

The authors are grateful to the Department of Chemistry, Shiraz University for support. The authors disclosed receipt of the following support for the research of this article: this work was

supported by the Iran High-Tech Laboratory Network [grant number: 29810 LabsNet]. Sašo Gyergyek acknowledge the financial support from the Slovenian Research Agency (research core funding No. P2–0089). The authors also acknowledge the Centre of Excellence in Nanoscience and Nanotechnology – Nanocenter for the use of the Jeol JEM-2100 transmission electron microscope.

References

1 W. Al Zoubi and Y. G. Ko, *J. Organomet. Chem.*, 2016, **822**, 173–188.
2 A. Erxleben, *Inorg. Chim. Acta*, 2018, **472**, 40–57.
3 M. T. Kaczmarek, M. Zabiszak, M. Nowak and R. Jastrzab, *Coord. Chem. Rev.*, 2018, **370**, 42–54.
4 L. Lecarme, L. Chiang, J. Moutet, N. Leconte, C. Philouze, O. Jarjayes, T. Storr and F. Thomas, *Dalton Trans.*, 2016, **45**, 16325–16334.
5 X. Ran, L. Wang, Y. Lin, J. Hao and D. Cao, *Appl. Organomet. Chem.*, 2010, **24**, 741–747.
6 S. Rana, J. P. Biswas, A. Sen, M. Clémancey, G. Blondin, J.-M. Latour, G. Rajaraman and D. Maiti, *Chem. Sci.*, 2018, **9**, 7843–7858.
7 H. L. Singh, *Res. Chem. Intermed.*, 2011, **37**, 1087–1101.
8 M. More, P. Joshi, Y. Mishra and P. Khanna, *Mater. Today Chem.*, 2019, **14**, 100195.
9 A. Nishinaga, H. Ohara, H. Tomita and T. Matsuura, *Tetrahedron Lett.*, 1983, **24**, 213–216.
10 A. P. Vieira, C. A. Wegermann and A. M. D. C. Ferreira, *New J. Chem.*, 2018, **42**, 13169–13179.
11 A. A. Emara and A. A. Abou-Hussen, *Spectrochim. Acta, Part A*, 2006, **64**, 1010–1024.
12 M. R. Maurya, N. Jangra, F. Avecilla and I. Correia, *Eur. J. Inorg. Chem.*, 2019, **2019**, 314–329.
13 M. Sutradhar, M. A. Andrade, S. A. Carabineiro, L. M. Martins, M. d. F. C. Guedes da Silva and A. J. Pombeiro, *Nanomater.*, 2021, **11**, 1456.
14 P. G. Cozzi, *Chem. Soc. Rev.*, 2004, **33**, 410–421.
15 E. M. McGarrigle and D. G. Gilheany, *Chem. Rev.*, 2005, **105**, 1563–1602.
16 M. Lashanizadegan and Z. Zareian, *Catal. Lett.*, 2011, **141**, 1698–1702.
17 S. K. Maiti, S. Dinda, M. Nandi, A. Bhaumik and R. Bhattacharyya, *J. Mol. Catal. A: Chem.*, 2008, **287**, 135–141.
18 M. R. Maurya, A. K. Chandrakar and S. Chand, *J. Mol. Catal. A: Chem.*, 2007, **274**, 192–201.
19 S. More, S. Jadhav, R. Salunkhe and A. Kumbhar, *Mol. Catal.*, 2017, **442**, 126–132.
20 R. Ratti, S. Kaur, M. Vaultier and V. Singh, *Catal. Commun.*, 2010, **11**, 503–507.
21 K. B. Sidhpuria, A. L. Daniel-da-Silva, T. Trindade and J. A. Coutinho, *Green Chem.*, 2011, **13**, 340–349.
22 G. Chouhan, D. Wang and H. Alper, *Chem. Commun.*, 2007, 4809–4811.
23 T. Hara, T. Kaneta, K. Mori, T. Mitsudome, T. Mizugaki, K. Ebitani and K. Kaneda, *Green Chem.*, 2007, **9**, 1246–1251.
24 V. Polshettiwar, R. Luque, A. Fihri, H. Zhu, M. Bouhrara and J.-M. Basset, *Chem. Rev.*, 2011, **111**, 3036–3075.
25 V. Polshettiwar and R. S. Varma, *Green Chem.*, 2010, **12**, 743–754.
26 E. Rafiee and S. Eavani, *Green Chem.*, 2011, **13**, 2116–2122.
27 M. A. Zolfigol, V. Khakyzadeh, A. R. Moosavi-Zare, A. Rostami, A. Zare, N. Iranpoor, M. H. Beyzavi and R. Luque, *Green Chem.*, 2013, **15**, 2132–2140.
28 W. A. Duetz, J. B. Van Beilen and B. Witholt, *Curr. Opin. Biotechnol.*, 2001, **12**, 419–425.
29 N. A. M. Fadzil, M. H. A. Rahim and G. P. Maniam, *Chin. J. Catal.*, 2014, **35**, 1641–1652.
30 F. Löbermann, P. Mayer and D. Trauner, *Angew. Chem., Int. Ed.*, 2010, **49**, 6199–6202.
31 N. Viswanadham, S. K. Saxena and H. Ala'a, *Mater. Today Chem.*, 2017, **3**, 37–48.
32 C. Zhu, J.-X. Liang, Y. Meng, J. Lin and Z. Cao, *Chin. J. Catal.*, 2021, **42**, 1030–1039.
33 P. Mohammadpour and E. Safaei, *RSC Adv.*, 2020, **10**, 23543–23553*Synfacts*, 2020, **16**(09), 1088.
34 M. Sankaralingam, M. Balamurugan and M. Palaniandavar, *Coord. Chem. Rev.*, 2020, **403**, 213085.
35 M. Mirzaee, B. Bahramian and M. Mirebrahimi, *Chin. J. Catal.*, 2016, **37**, 1263–1274.
36 P. Spannring, P. C. Bruijnincx, B. M. Weckhuysen and R. J. K. Gebbink, *Catal. Sci. Technol.*, 2014, **4**, 2182–2209.
37 Y. Tao, O. De Luca, B. Singh, A. J. Kamphuis, J. Chen, P. Rudolf and P. P. Pescarmona, *Mater. Today Chem.*, 2020, **18**, 100373.
38 G. Urgoitia, R. SanMartin, M. T. Herrero and E. Domínguez, *ACS Catal.*, 2017, **7**, 3050–3060.
39 C. Lin and L. Shen, *ChemCatChem*, 2019, **11**, 961–968.
40 D. B. Miklos, C. Remy, M. Jekel, K. G. Linden, J. E. Drewes and U. Hübner, *Water Res.*, 2018, **139**, 118–131.
41 D. Saini, R. Aggarwal, S. Anand, N. Satrawala, R. Joshi and S. Sonkar, *Mater. Today Chem.*, 2020, **16**, 100256.
42 D. Wang, J. R. Gardinier and S. V. Lindeman, *Dalton Trans.*, 2019, **48**, 14478–14489.
43 H. Jiang, H. Gong, Z. Yang, X. Zhang and Z. Sun, *React. Kinet. Catal. Lett.*, 2002, **75**, 315–321.
44 P. Daw, R. Petakamsetty, A. Sarbajna, S. Laha, R. Ramapanicker and J. K. Bera, *J. Am. Chem. Soc.*, 2014, **136**, 13987–13990.
45 R. Noyori, M. Aoki and K. Sato, *Chem. Commun.*, 2003, 1977–1986.
46 R. Willand-Charnley, T. J. Fisher, B. M. Johnson and P. H. Dussault, *Org. Lett.*, 2012, **14**, 2242–2245.
47 R. Sattar, R. Mukhtar, M. Atif, M. Hasnain and A. Irfan, *J. Heterocycl. Chem.*, 2020, **57**, 2079–2107.
48 B. Jiang, T. Rajale, W. Wever, S. J. Tu and G. Li, *Chem.–Asian J.*, 2010, **5**, 2318–2335.
49 F. Bahrami, F. Panahi, F. Daneshgar, R. Yousefi, M. B. Shahsavani and A. Khalafi-Nezhad, *RSC Adv.*, 2016, **6**, 5915–5924.
50 M. M. Heravi, E. Hashemi, Y. S. Beheshtiha, K. Kamjou, M. Toolabi and N. Hosseintash, *J. Mol. Catal. A: Chem.*, 2014, **392**, 173–180.

51 S. K. Alla, P. Sadhu and T. Punniyamurthy, *J. Org. Chem.*, 2014, **79**, 7502–7511.
52 N. Khatun, S. Guin, S. K. Rout and B. K. Patel, *RSC Adv.*, 2014, **4**, 10770–10778.
53 A. R. Tiwari and B. M. Bhanage, *Org. Biomol. Chem.*, 2016, **14**, 7920–7926.
54 L. Wang, Z.-G. Ma, X.-J. Wei, Q.-Y. Meng, D.-T. Yang, S.-F. Du, Z.-F. Chen, L.-Z. Wu and Q. Liu, *Green Chem.*, 2014, **16**, 3752–3757.
55 H.-Z. Xie, Q. Gao, Y. Liang, H.-S. Wang and Y.-M. Pan, *Green Chem.*, 2014, **16**, 2132–2135.
56 D. Yang, X. Zhu, W. Wei, N. Sun, L. Yuan, M. Jiang, J. You and H. Wang, *RSC Adv.*, 2014, **4**, 17832–17839.
57 F. Zhu, J.-L. Tao and Z.-X. Wang, *Org. Lett.*, 2015, **17**, 4926–4929.
58 S. Ojala, N. Koivikko, T. Laitinen, A. Mouammine, P. K. Seelam, S. Laassiri, K. Ainassaari, R. Brahmi and R. L. Keiski, *Catalysts*, 2015, **5**, 1092–1151.
59 S. Scirè and L. F. Liotta, *Appl. Catal., B*, 2012, **125**, 222–246.
60 M. Zarghani and B. Akhlaghinia, *RSC Adv.*, 2016, **6**, 38592–38601.
61 S. Fan, W. Dong, X. Huang, H. Gao, J. Wang, Z. Jin, J. Tang and G. Wang, *ACS Catal.*, 2017, **7**, 243–249.
62 M. Arshadi and M. Ghiaci, *Appl. Catal., A*, 2011, **399**, 75–86.
63 Y. Kuwahara, Y. Yoshimura and H. Yamashita, *Catal. Sci. Technol.*, 2016, **6**, 442–448.
64 S. Samanta and R. Srivastava, *Appl. Catal., B*, 2017, **218**, 621–636.
65 Y. Zhang, L. Zhao, H. Zhang, R. Huang and J. Zhao, *Appl. Organomet. Chem.*, 2017, **31**, e3709.
66 L. Fu, S. Zhao, Y. Chen and Z. Liu, *Chem. Commun.*, 2016, **52**, 5577–5580.
67 R. Neumann and C. Abu-Gnim, *J. Am. Chem. Soc.*, 1990, **112**, 6025–6031.
68 Y. Deng, Z. Ma, K. Wang and J. Chen, *Green Chem.*, 1999, **1**, 275–276.
69 R. Dileep and B. Rudresha, *RSC Adv.*, 2015, **5**, 65870–65873.
70 Z. Saedi, S. Tangestaninejad, M. Moghadam, V. Mirkhani and I. Mohammadpoor-Baltork, *Catal. Commun.*, 2012, **17**, 18–22.
71 S. Jarupinthusophon, U. Thong-In and W. Chavasiri, *J. Mol. Catal. A: Chem.*, 2007, **270**, 289–294.
72 V. Kumar, V. P. Reddy, R. Sridhar, B. Srinivas and K. R. Rao, *Synlett*, 2009, **2009**, 739–742.
73 E. Safaei, Z. Alaji, F. Panahi, A. Wojtczak and J. Z. Jagličić, *New J. Chem.*, 2018, **42**, 7230–7236.
74 H. Sharghi, J. Aboonajmi and M. Aberi, *J. Org. Chem.*, 2020, **85**, 6567–6577.
75 X. Fan, Y. He, Y. Wang, X. Zhang and J. Wang, *Chin. J. Chem.*, 2011, **29**, 773–777.
76 R. D. Jana, A. Das and T. K. Paine, *Inorg. Chem.*, 2021, **60**, 5969–5979.
77 J. L. Lee, D. L. Ross, S. K. Barman, J. W. Ziller and A. S. Borovik, *Inorg. Chem.*, 2021, **60**, 13759–13783.
78 M. Guo, T. Corona, K. Ray and W. Nam, *ACS Cent. Sci.*, 2018, **5**, 13–28.
79 T. Karimpour, E. Safaei and B. Karimi, *RSC Adv.*, 2019, **9**, 14343–14351; *Synfacts*, **15**, 0918.
80 A. Gonzalez-de-Castro and J. Xiao, *J. Am. Chem. Soc.*, 2015, **137**, 8206–8218.
81 H. Yuan, W.-J. Yoo, H. Miyamura and S. Kobayashi, *J. Am. Chem. Soc.*, 2012, **134**, 13970–13973.
82 D. Xu, W. Wang, C. Miao, Q. Zhang, C. Xia and W. Sun, *Green Chem.*, 2013, **15**, 2975–2980.
83 H. Sharghi, M. Aberi and M. M. Doroodmand, *Adv. Synth. Catal.*, 2008, **350**, 2380–2390.
84 J. Javidi, M. Esmaeilpour and M. R. Khansari, *RSC Adv.*, 2015, **5**, 73268–73278.